A&A 388, 1022–1035 (2002)
DOI: 10.1051/0004-6361:20020488

Astronomy & Astrophysics

Thermal properties of magnetic flux tubes

I. Solution of the diffusion problem

F. Moreno-Insertis[1,2], M. Schüssler[3], and K. Glampedakis[4]

[1] Instituto de Astrofísica de Canarias, 38200 La Laguna (Tenerife), Spain
e-mail: fmi@ll.iac.es
[2] Dept of Astrophysics, Universidad de La Laguna, 38200 La Laguna, Spain
[3] Max-Planck-Institut für Aeronomie, Max-Planck-Str. 2, 37191 Katlenburg-Lindau, Germany
e-mail: schuessler@linmpi.mpg.de
[4] Dept of Physics and Astronomy, Cardiff University, Cardiff CF24 3YB, UK

Received 13 November 2001 / Accepted 27 March 2002

Abstract. The heat flow and temperature structure within and surrounding a magnetic flux tube stored in mechanical equilibrium in a stellar convection zone are considered. The stationary thermal equilibrium state is determined through the analytical solution of a two-dimensional heat diffusion problem for an infinitely long cylinder with different thermal conductivities inside and outside the cylinder, both spatially variable. In the exterior of the cylinder, convective heat transport is approximated in terms of a linear diffusive process, while in its interior convection is assumed to be suppressed and only the much smaller radiative conductivity remains. The results show that, under the conditions prevailing near the bottom of the solar convection zone and in the limit of small cylinder radius, the temperature disturbance (thermal shadow) in the exterior of the insulating cylinder is almost negligible due to the large effiency of convective energy transport. The spatial dependence of the conductivities and the curvature of the external temperature profile lead to a *temperature excess* in the interior with respect to the undisturbed temperature profile far away from the cylinder. We show that, within the framework of the thin magnetic flux tube approximation, this temperature excess is due to a heating term equal to the negative divergence of the undisturbed radiative heat flow, as suggested earlier by Fan & Fisher (1996). These results are independent of the treatment of the convective transport in the exterior as long as the stratification is almost adiabatic. The consequences for the storage of magnetic flux in the solar convection zone, brought about by the enhanced buoyancy and caused by the heating effect, are discussed.

Key words. Sun: magnetic fields – Sun: interior

1. Introduction

The operation of a hydromagnetic dynamo as a generator for the solar magnetic cycle requires the storage of magnetic flux near the bottom of the convection zone for times comparable with the cycle (half) period of 11 years (Parker 1975; Spruit & van Ballegooijen 1982; Schüssler 1983). While fields with a strength below the equipartition value with respect to convection ($\lesssim 10^4$ G) may be pumped toward the bottom of the convection zone (e.g., Tobias et al. 1998), the much stronger fields in the order of 10^5 G indicated by stability analysis and numerical simulations of rising flux tubes (Moreno-Insertis 1986, 1992; Choudhuri & Gilman 1987; D'Silva & Choudhuri 1993; Fan et al. 1994; Schüssler et al. 1994; Caligari et al. 1995, 1998) require the establishment of a mechanical equilibrium (see also Rempel et al. 2000). Moreno-Insertis et al. (1992) have shown that magnetic flux can be stored in the form of toroidal flux tubes (flux rings) in mechanical equilibrium within a subadiabatically stratified layer of convective overshoot below the convection zone proper. This equilibrium is characterised by (a) neutral buoyancy (density inside the tube equal to the external density) and (b) balance between the magnetic curvature and Coriolis forces. An initially buoyant flux tube reaches the state of neutral buoyancy by rising in the overshoot layer: the stable (subadiabatic) stratification leads to a temperature deficit of the flux tube with respect to its surroundings and a concomitant reduction of its buoyancy until the state of neutral buoyancy is attained.

The temperature deficit necessary for neutral buoyancy $(\Delta T)_{\rm B}/T \simeq 1/\beta$ (β: ratio of gas pressure to magnetic pressure) is very small near the bottom of the convection zone. Even for a field of 10^5 G we only have

$(\Delta T)_{\rm B} \simeq 20$ K, while the ambient temperature is about 2×10^6 K. Convective energy transport is suppressed by such a strong magnetic field, but radiative transport remains and tends to smooth out the temperature deficit in a neutrally buoyant flux tube (Moreno-Insertis 1983). The time scale of this process is the radiative diffusion time, $\tau_{\rm r} = R^2/\chi_{\rm T}$, where R is the radius of the flux tube and $\chi_{\rm T}$ is the radiative thermal diffusion coefficient. Near the bottom of the convection zone we have $\chi_{\rm T} \simeq 10^7$ cm^2 s^{-1} (e.g. Spruit 1977b), so that for a flux tube radius of 1000 km (corresponding to a magnetic flux of about 3×10^{21} Mx for a field strength of 10^5 G) we find $\tau_{\rm r} \simeq 30$ yr. Consequently, flux tubes stored in the overshoot layer for a few years would seem to be barely affected by radiative diffusion.

On the other hand, we observe that $(\Delta T)_{\rm B}$ for neutral buoyancy is much smaller than the variation of the external temperature over the cross section of a horizontal flux tube: for a tube radius of 1000 km we obtain a temperature difference of $\Delta T_{\rm e} \simeq 2 \times 10^4$ K between the top and the bottom of the flux tube. Consequently, the buoyancy of a flux tube is strongly affected if the internal temperature only changes by a small fraction of the external temperature *variation* over the flux tube diameter. This indicates that it may not suffice to consider only the zeroth-order approximation in tube radius of the radiative energy exchange between the flux tube and its exterior. Higher-order effects depending on the actual height profile of the external temperature should also be taken into account. As we show in this paper, such effects may arise from the radial variation of the gravitational acceleration, from spatial variation of the convective and radiative thermal conductivities, and from thermal shadows (Parker 1984b, 1987).

A first step along these lines was taken by Fan & Fisher (1996, hereafter referred to as FF96), who suggested that a magnetic flux tube with internally suppressed convective energy transport, experiences a net heating due to a non-vanishing divergence of the external radiative heat flow, provided that radiative transport is unaffected within the flux tube. The amount of heating for conditions prevailing near the bottom of the solar convection zone appears to be large enough to have considerable consequences for the storage of magnetic flux tubes. The validity of the claim in FF96 cannot be fully assessed from the paper since it gives neither a formal solution of the diffusion problem nor a full analysis of the asymptotic behaviour in the limit of the small flux tube radius. In order to clarify this situation, we have carried out, in the framework of a diffusion model, a detailed study of the thermal state of a magnetic flux tube embedded in a medium pervaded by a fixed energy flux at a large distance from the flux tube. In particular, we have considered the effects of (a) different thermal transport coefficients inside and outside the flux tube, (b) spatially varying transport coefficients, and (c) convective transport proportional to the gradient of potential temperature.

Section 2 gives the analytical solution of the stationary heat flow problem. In Sect. 3 we present results of a numerical simulation of the time-dependent problem in order to provide some understanding of the manner in which the stationary solution is approached and the associated time scales. Section 4 contains the description of both the stationary and the time-dependent problem in the framework of the thin flux tube approximation for the case of a fixed external temperature field (no thermal shadow). Quantitative estimates and the consequences for the storage of flux tubes near the bottom of the solar convection zone are considered in Sect. 5. Section 6 contains a summary and discussion of the results.

2. Stationary heat flow through a poorly conducting cylinder in a non-uniform medium

2.1. Heat transfer equation

In this section we consider the stationary temperature distribution resulting after the introduction of an imperfectly insulating cylinder in a medium with radiative or convective heat transport. We assume the unperturbed state to be a plane-parallel stratified medium, which fulfils a stationary heat transfer equation of the form

$$\nabla \cdot \boldsymbol{F}_0 = 0, \tag{1}$$

where the unperturbed heat flow vector is denoted by $\boldsymbol{F}_0$. It has only a vertical (z) component, F_0, with a radiative and a convective part, i.e.,

$$\begin{aligned} F_0 &= F_{0,\rm rad} + F_{0,\rm conv} \\ &= -\kappa_{\rm r}(z)\,\frac{{\rm d}T_0}{{\rm d}z} - \kappa_{\rm c}(z)\left[\frac{{\rm d}T_0}{{\rm d}z} - \left(\frac{{\rm d}T}{{\rm d}z}\right)_{\rm ad}\right]. \end{aligned} \tag{2}$$

Here $T_0(z)$ is the unperturbed temperature profile, $\kappa_{\rm r} = 16\sigma T_0^3/3\bar{k}\rho$ is the radiative thermal conductivity (σ: Stefan-Boltzmann constant, $\bar{k}$: Rosseland mean opacity, $c_{\rm p}$ specific heat per unit volume), $\kappa_{\rm c}$ is the convective transport coefficient for a linearized dependence of the convective flux on the superadiabatic temperature gradient (Spruit 1977a), and $({\rm d}T/{\rm d}z)_{\rm ad}$ is the adiabatic temperature gradient. The description of the energy transport in Eq. (2) uses the diffusion approximation for the radiative transfer and a linearized mixing length approach for convection (i.e., the convective flux is proportional to the gradient of *potential* temperature).

We now consider the perturbation caused by the presence of a partially insulating, infinite cylinder of radius R, whose axis points in the horizontal direction. For simplicity we make the axis of the cylinder coincide with the y coordinate axis. We assume the heat transport within the cylinder to be purely radiative with a spatially dependent conductivity $\kappa_{\rm i}(\boldsymbol{r})$, so that the heat flow vector inside is given by

$$\boldsymbol{F}_{\rm i} = -\kappa_{\rm i}(\boldsymbol{r})\,\nabla T_{\rm i}, \tag{3}$$

with $T_{\rm i}(\boldsymbol{r})$ the internal temperature. In the stationary state, the temperature distribution obeys the equation

$$\nabla \cdot [\kappa_{\rm i}(\boldsymbol{r})\,\nabla T_{\rm i}] = 0. \tag{4}$$

The presence of the cylinder causes a temperature perturbation $T'_{\rm e}(\boldsymbol{r}) = T(\boldsymbol{r}) - T_0(z)$ in the external medium, so that the temperature gradient no longer always points in the vertical direction. A non-vanishing horizontal component of the heat flow results, which is carried in the exterior by radiative transfer and by turbulent transport described by the convective transport coefficient, $\kappa_{\rm c}$. Assuming no variation in the y-direction (along the infinite cylinder), the relation between the perturbed heat flow, $\boldsymbol{F}$, and the perturbed temperature profile in the medium outside the cylinder, $T(\boldsymbol{r}) = T_0(z) + T'_{\rm e}(\boldsymbol{r})$, is given by:

$$\begin{aligned}\boldsymbol{F} &= -\kappa_{\rm r}\,\nabla T - \kappa_{\rm c}\left[\frac{\partial T}{\partial z} - \left(\frac{{\rm d}T}{{\rm d}z}\right)_{\rm ad}\right]\boldsymbol{e}_z - \kappa_{\rm c}\frac{\partial T}{\partial x}\,\boldsymbol{e}_x \\ &= \boldsymbol{F}_0 - \kappa\,\nabla T'_{\rm e}\,, \end{aligned} \tag{5}$$

where we have written $\kappa \equiv \kappa_{\rm r} + \kappa_{\rm c}$. Here, $\boldsymbol{e}_x$ and $\boldsymbol{e}_z$ are the unit vectors in the x- and the z-direction, respectively, and Eq. (2) has been used in order to obtain the second equality. We have assumed (following Spruit 1977a) that the convective energy transport in the horizontal direction can be described by turbulent diffusion with $\kappa_{\rm c}$ as the effective thermal conductivity. We have also assumed that the thermal conductivities and $({\rm d}T/{\rm d}z)_{\rm ad}$ are unaffected by the temperature perturbation. We briefly discuss the consequences of relaxing this assumption at the end of Sect. 4. In the stationary state we have $\nabla \cdot \boldsymbol{F} = 0$ and, using Eq. (1), we obtain an equation for the perturbation $T'_{\rm e}$ in the external medium, viz.

$$\nabla \cdot [\kappa(z)\,\nabla T'_{\rm e}] = 0. \tag{6}$$

Both Eq. (6) for the external and Eq. (4) for the internal temperature are of diffusion type. To solve the full problem we require the temperature and the normal component of the heat flow to be continuous at the boundary between cylinder and external medium (at $r = R$ in polar coordinates centered at the cylinder axis):

$$T_0 + T'_{\rm e} = T_{\rm i}, \tag{7}$$

$$(\boldsymbol{F}_0 - \kappa\,\nabla T'_{\rm e}) \cdot \boldsymbol{e}_{\rm n} = (-\kappa_{\rm i}\,\nabla T_{\rm i}) \cdot \boldsymbol{e}_{\rm n}, \tag{8}$$

where $\boldsymbol{e}_{\rm n}$ is the normal vector at the surface of the cylinder. We also require the heat flow perturbation to vanish asymptotically far from the cylinder, viz.

$$\kappa(z)\,\nabla T'_{\rm e} \to 0 \qquad \text{for} \qquad r \to \infty. \tag{9}$$

Finally, the internal temperature, $T_{\rm i}$, has to be regular at the axis of the cylinder ($r = 0$).

2.2. Exponential profiles of the conductivity coefficients: Formal solution

There is no general solution of Eqs. (4) and (6) for arbitrary spatial distribution of the conductivity coefficients. An analytical solution can be obtained in the case of exponential profiles for κ and $\kappa_{\rm i}$, namely:

$$\kappa(z) = \kappa_0\,\exp(Mz), \tag{10}$$

$$\kappa_{\rm i}(z) = \kappa_{\rm i0}\,\exp(M_{\rm i}z). \tag{11}$$

This *ansatz* may restrict the generality of the results, but to a lesser extent than could be thought at first sight. On the one hand, (1) in the convection zone and overshoot region $\kappa_{\rm r} \ll \kappa_{\rm c}$ holds, so that the spatial variation of $\kappa_{\rm r}$ can be neglected in the external medium, and (2) in the radiative interior, $\kappa_{\rm c}$ vanishes. On the other hand, the calculation in the limit of the thin flux tube approximation (presented in Sect. 4) shows that only the first derivatives of κ and $\kappa_{\rm i}$ matter. Therefore, in that limit, any height dependence of the transport coefficients can be locally approximated by Eqs. (10) and (11). We define

$$\Theta(r,\phi) \stackrel{\rm def}{=} \sqrt{\kappa(r,\phi)}\;T'_{\rm e}(r,\phi), \tag{12}$$

$$\Xi(r,\phi) \stackrel{\rm def}{=} \sqrt{\kappa_{\rm i}(r,\phi)}\;T_{\rm i}(r,\phi). \tag{13}$$

Inserting this into Eqs. (4) and (6) we obtain equations of the Helmholtz type for evanescent waves, viz.

$$-\frac{M^2}{4}\,\Theta + \Delta\,\Theta = 0 \qquad (r \geq R), \tag{14}$$

$$-\frac{M_{\rm i}^2}{4}\,\Xi + \Delta\,\Xi = 0 \qquad (r \leq R). \tag{15}$$

These equations can be solved in terms of a Fourier series including the modified Bessel functions $\mathcal{K}_m(Mr/2)$ and $\mathcal{I}_m(M_{\rm i}r/2)$. To satisfy the boundary conditions at $r \to \infty$ in the external medium and at $r \to 0$ in the interior of the cylinder, we have to choose the $\mathcal{K}_m$ functions outside and the $\mathcal{I}_m$ inside. Using the definitions

$$a \stackrel{\rm def}{=} \frac{MR}{2}, \quad a_{\rm i} \stackrel{\rm def}{=} \frac{M_{\rm i}R}{2}, \tag{16}$$

$$\hat{r} \stackrel{\rm def}{=} \frac{Mr}{2}, \quad \hat{r}_{\rm i} \stackrel{\rm def}{=} \frac{M_{\rm i}r}{2}, \tag{17}$$

we can write the solutions for $T'_{\rm e}$ in the external medium and for T in the internal medium as:

$$T'_{\rm e}(r,\phi) = \exp(-\hat{r}\cos\phi)\;\sum_{m=0}^{\infty} G_m \frac{\mathcal{K}_m(\hat{r})}{\mathcal{K}_m(a)}\;\cos(m\phi) \qquad \text{for } (r \geq R), \tag{18}$$

$$T_{\rm i}(r,\phi) = \exp(-\hat{r}_{\rm i}\cos\phi)\;\sum_{m=0}^{\infty} H_m \frac{\mathcal{I}_m(\hat{r}_{\rm i})}{\mathcal{I}_m(a_{\rm i})}\;\cos(m\phi) \qquad \text{for } (r \leq R). \tag{19}$$

The expansion coefficients G_m and H_m are determined by the matching conditions (7) and (8) at the interface between external medium and cylinder.

2.3. Matching of temperature and flux at the surface of the cylinder

The condition of continuity of the temperature at the boundary of the cylinder ($\hat{r} = a, \hat{r}_\mathrm{i} = a_\mathrm{i}$), Eq. (7), becomes:

$$T_0(R,\phi) + \exp\left(-a\cos\phi\right) \sum_{m=0}^{\infty} G_m \cos(m\phi) = \exp\left(-a_\mathrm{i}\cos\phi\right) \sum_{m=0}^{\infty} H_m \cos(m\phi). \quad (20)$$

The condition for the continuity of the normal heat flow component, Eq. (8), is less immediate to transform, since it involves the derivatives of the Bessel functions. We make use of the recurrence relation for the derivatives $\mathcal{K}'_m$ and $\mathcal{I}'_m$ as follows:

$$z\,\mathcal{K}'_m(z) = -z\,\mathcal{K}_{m+1}(z) + m\,\mathcal{K}_m(z), \quad (21)$$

$$z\,\mathcal{I}'_m(z) = z\,\mathcal{I}_{m+1}(z) + m\,\mathcal{I}_m(z). \quad (22)$$

Using these relations in Eq. (8), we obtain the following condition:

$$2a\delta T\cos\phi + \exp(a\cos\phi) \times \sum_{m=0}^{\infty} G_m \left[a\cos\phi - m + a\,\frac{\mathcal{K}_{m+1}(a)}{\mathcal{K}_m(a)}\right]\cos(m\phi) = \frac{\kappa_{\mathrm{i}0}}{\kappa_0}\exp(a_\mathrm{i}\cos\phi) \times \sum_{m=0}^{\infty} H_m \left[a_\mathrm{i}\cos\phi - m - a_\mathrm{i}\,\frac{\mathcal{I}_{m+1}(a_\mathrm{i})}{\mathcal{I}_m(a_\mathrm{i})}\right]\cos(m\phi), \quad (23)$$

where

$$\delta T \stackrel{\mathrm{def}}{=} \frac{F_0}{\kappa_0 M}. \quad (24)$$

2.4. Limit of small cylinder radius

There is no analytical solution of the matching conditions (20) and (23) for G_m and H_m in a general case. We thus go to the relevant limit in our problem, namely the case when the cylinder radius is small compared with the length scales of variation of the unperturbed temperature profile and of the heat transport coefficients, i.e., $|a| \ll 1$ and $|a_\mathrm{i}| \ll 1$. Under these conditions, we can use a simple Taylor expansion of the background temperature profile in the vicinity of the cylinder:

$$T_0(z) = T_{\mathrm{e}0} + Qz + Pz^2. \quad (25)$$

On the surface of the cylinder $z = R\cos\phi$, so that we have

$$T_0(z) = T_{\mathrm{e}0} + 2a^2\frac{P}{M^2} + 2a\frac{Q}{M}\cos\phi + 2a^2\frac{P}{M^2}\cos 2\phi. \quad (26)$$

In the following, P and Q are taken as fixed quantities determined by a given model of the unperturbed stratification which satisfies Eq. (1).

We expand the matching conditions for the temperature, Eq. (20), and flux, Eq. (23), in powers of a and a_i and retain terms up to a^2 and a_i^2. At the same time, we truncate the Fourier series at the $\cos(2\phi)$ terms. We then equate the coefficients of each $\cos(m\,\phi)$ term on both sides of Eq. (20) and perform the same operation for Eq. (23). Six algebraic equations for the coefficients G_0, G_1, G_2, H_0, H_1, and H_2 are thus obtained, from which the temperature disturbance inside and outside the cylinder can be determined. Details of this operation are given in Appendix A.

2.5. Temperature perturbation for a strongly insulating cylinder

In order to illustrate the various effects influencing the thermal structure more clearly, we consider the case of a strongly insulating cylinder, $\kappa_{\mathrm{i}0} \ll \kappa_0$, in an environment dominated by convective energy transport, $F_{0,\mathrm{rad}} \ll F_{0,\mathrm{conv}}$. The latter assumption is satisfied for $|\kappa_{\mathrm{i}0}Q| \ll F_0$. Under these conditions, the excess temperature in the tube interior, $T'_\mathrm{i} \stackrel{\mathrm{def}}{=} T_\mathrm{i} - T_0$, is given by

$$T'_\mathrm{i}(r,\phi) = \frac{1}{2}\left(PR^2 + QRa_\mathrm{i} - \Delta T\,a_\mathrm{i}\right)\left(1 - \frac{r^2}{R^2}\right) - \Delta T\frac{r}{R}\cos\phi + \Delta T\,a\left[\frac{1}{2} - \gamma - \ln\left(\frac{a}{2}\right) + \frac{r^2}{R^2}\cos 2\phi\right] \quad (27)$$

where

$$\Delta T \stackrel{\mathrm{def}}{=} 2a\delta T = \frac{F_0 R}{\kappa_0}, \quad (28)$$

and $\gamma = 0.577\ldots$ is Euler's constant. The corresponding expression for the external temperature perturbation in the vicinity of the cylinder (more precisely, for $a \le \hat{r} \ll 1$) is

$$T'_\mathrm{e}(r,\phi) = -\Delta T\,\frac{R}{r}\cos\phi + \Delta T\,a\left[\frac{1}{2} - \gamma - \ln\left(\frac{\hat{r}}{2}\right) + \frac{1}{2}\left(1 + \frac{R^2}{r^2}\right)\cos 2\phi\right]. \quad (29)$$

Most of the terms in Eqs. (27) and (29) are proportional to ΔT. As defined in (28), ΔT is a measure of the temperature difference across a distance of order the cylinder radius that is necessary to carry the whole heat flow F_0 by means of the conductivity κ_0. A strongly insulating cylinder blocks the heat flow in its interior and causes a perturbation in a region of size R around itself. Hence, ΔT also provides a measure for the temperature perturbation we can expect around the cylinder. Equations (27) and (29) thus contain terms relating to the *thermal shadows* around the tube as well as terms relating to the unperturbed thermal distribution (the latter only in Eq. (27)). We analyze both kinds of terms in the following.

The two kinds of terms in the expressions for the temperature perturbation come from different physical

effects. The terms containing the parameters P and Q in Eq. (27), viz.

$$\frac{1}{2}\left(PR^2 + QRa_\mathrm{i}\right)\left(1 - \frac{r^2}{R^2}\right) \tag{30}$$

correspond to the temperature perturbation that would be established within the cylinder if the temperature on its periphery were *prescribed* to be equal to the unperturbed temperature profile given by Eq. (26) (i.e., the internal temperature perturbation in the absence of any thermal shadow). This can be shown explicitly by solving the general problem of Eq. (4) with boundary condition as given in Eq. (26) using an expansion in terms of Bessel functions as in Eq. (19), and then applying the limit $a_\mathrm{i} \ll 1$. The same result is obtained in the case of the thin flux tube approximation studied in Sect. 4. In the simple case when the conductivity inside is constant (i.e., if $a_\mathrm{i} \to 0$), only the P-term remains. This can be readily understood in terms of the elementary potential theory: if κ_i is constant, the linear term in the temperature distribution is identical inside as outside; a correction is necessary only for the parabolic P-term. On the other hand, if the conductivity inside is non-homogeneous, then an additional term appears (the Q-term in Eq. (30)) which accounts for the fact that it is easier to create a heat flow at the top of the cylinder than at the bottom (or vice versa, depending on the sign of M_i).

The remaining terms in Eq. (27) i.e., all terms containing the factor ΔT, as well as the whole expression (29), correspond to thermal perturbations associated with the diversion of the heat flow around the insulating cylinder. In the special case of Eqs. (27) and (29) these perturbations amount to a cool *thermal shadow* at the rear and a *hot spot* at its front (*front* and *rear* are meant in this paper *as seen by the incoming total heat flow*. The heat flow impinges on the tube at its front and leaves it at the rear). In fact, the term proportional to $\Delta T \cos\phi$ in both equations is the classical thermal shadow term in the simple problem of a strongly insulating cylinder inserted in a conducting medium with constant conductivity coefficients inside and outside. The other ΔT-terms in those equations result from the spatial inhomogeneity of κ_i and κ: the thermal shadow at the rear of the tube must be larger if the conductivity there is smaller, and vice versa for the hot spot. Figure 1 illustrates the spatial distribution of the temperature perturbation within and in the vicinity of the cylinder for a case dominated by thermal shadow and hot spot.

If the radiative flux outside the cylinder is non-negligible, the expressions for the temperature perturbations become more complicated (see Appendix A). In a region of convective overshoot, for instance, the convective heat flow is *antiparallel* to the total heat flow vector and the radiative flux is larger than the undisturbed heat flow. As a result, the presence of the cylinder in that case leads to a cool thermal shadow *at the front side* and a hot spot *at the rear side* of the cylinder. For the deep solar convection zone, however, we show in Sect. 5 that the effects of thermal shadows and hot spots in any case are much smaller than the terms due to the curvature of the undisturbed temperature profile (the term proportional to P in Eq. (27)) and the spatial variation of κ_i (the term proportional to Q). This leads to negligible external temperature perturbations and a cylindrically symmetric internal perturbation given by Eq. (30).

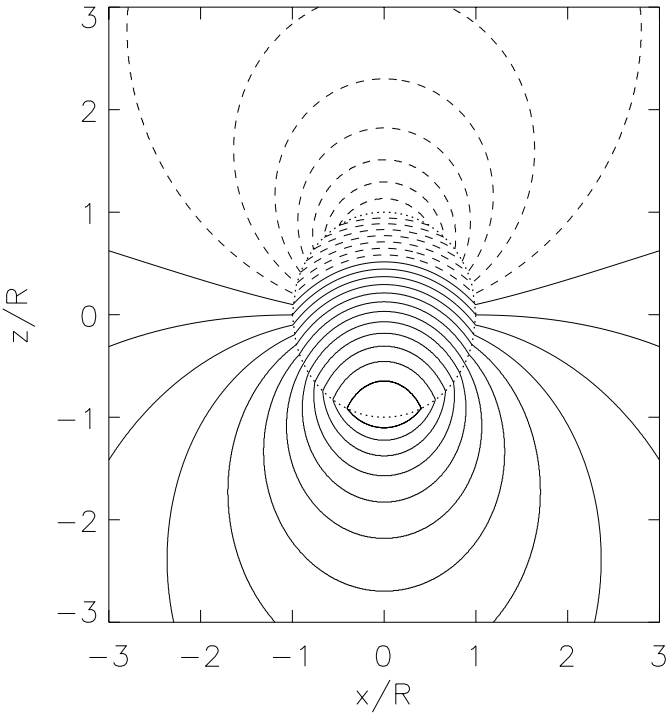

Fig. 1. Isolines of the temperature perturbation within and outside the cylinder for $P > 0$, $M > 0$, $M_\mathrm{i} < 0$, and $\kappa_{\mathrm{i}0} \ll \kappa_0$. Solid lines correspond to positive values, dashed lines to negative values. The dotted line indicates the periphery of the cylinder. The undisturbed heat flow vector is directed upward, in the positive z-direction. The hot spot below the cylinder is stronger than the thermal shadow above because the external conductivity increases with height. The region of positive temperature perturbation dominates even more markedly within the cylinder since the internal conductivity decreases with height, leading to a flatter (steeper) temperature profile in the lower (upper) part of the cylinder.

2.6. Average temperature excess

To calculate the possible dynamical effects of the temperature perturbation in and around the thermally insulating cylinder one has to estimate the buoyancy ensuing in the cylinder from the temperature perturbation with respect to the unperturbed external medium. Given that the temperature perturbation is small (because the cylinder radius is small), the thermal buoyancy force per unit length of the cylinder, δF_B, can be simply calculated to first order of approximation as

$$\delta F_\mathrm{B} = \rho_0 g \int \frac{T_\mathrm{i}'}{T_{\mathrm{e}0}} \mathrm{d}A, \tag{31}$$

where g is the gravitational acceleration and the area integral is taken over the cross section of the cylinder. Consequently, the *average relative temperature excess,* $\langle \delta T_{\rm i} \rangle$, given by the integral in Eq. (31) divided by πR^2, is the relevant quantity that determines the total buoyancy force on the tube. In the limit $F_{0,\rm rad} \ll F_{0,\rm conv}$ considered in the previous subsection, this quantity is immediately calculated from Eq. (27). The result is:

$$\langle \delta T_{\rm i} \rangle = \frac{1}{4} \left(\frac{PR^2 + QRa_{\rm i}}{T_{\rm e0}} \right) + \frac{\Delta T}{T_{\rm e0}} \left[-\frac{a_{\rm i}}{4} + a \left(\frac{1}{2} - \gamma - \ln \frac{a}{2} \right) \right] . \quad (32)$$

We see that all terms have an R^2 dependence. Their relative size and, more importantly, the magnitude of the resulting temperature excess depend on the values of P, Q, a, and $a_{\rm i}$ corresponding to the situation considered.

3. The time-dependent problem: Numerical solutions

The stationary solution discussed in the previous section can only be established if the tube is held in place for at least a few times the characteristic timescale for thermal exchange with the surroundings. In an actual magnetic region in a stellar interior this thermal evolution can cause complicated dynamical processes which deform the magnetic tube (see Lenz et al. 2002). However, to understand the thermal properties of our system, it may be of interest at this point to disregard all kinematics and dynamics and study the time-dependent problem of the establishment of an equilibrium solution with heat conduction governed by an inhomogeneous diffusion coefficient which contains a strongly insulating cylindrical region.

To keep the problem as simple as possible, we adopt as an initial condition a one-dimensional temperature distribution in the whole domain which fulfills the condition of zero–divergence of the heat flow, viz.:

$$\nabla [\kappa(z) \nabla T_0(z)] = 0, \quad (33)$$

with the conductivity $\kappa(z)$ having an exponential profile as in Eq. (10). $T_0(z)$ then also has an exponential profile with constants determined by the boundary condition. Introducing a partially insulating cylinder in that atmosphere and calling $\tilde{\kappa}(x,z)$ the resulting conductivity function in the whole space, the thermal diffusion equation can be written:

$$\frac{\partial T(x,z,t)}{\partial t} = \nabla \left[\tilde{\chi}(x,z) \nabla T(x,z,t) \right] , \quad (34)$$

with

$$\tilde{\chi}(x,z) = \tilde{\kappa}(x,z)/c_{\rm p} \quad (35)$$

and $c_{\rm p}$ the specific heat per unit volume, which, for simplicity, has been assumed constant in deriving Eq. (34). We calculate the solution to the problem using a two-dimensional computer code which makes use of the ADI method (alternating direction implicit method) and contains an implementation of the Thomas algorithm for the solution of the resulting matrix equations. The scheme is semi-implicit and unconditionally stable. The integration box is a square with boundaries at $x = 0, 1$ and $z = 0, 1$. We choose $M = 1$ and $\kappa_0 = 1$ in Eq. (10). As boundary conditions we assume a constant and uniform heat flow of unit value pointing in the z-direction which enters the box at $z = 0$ and leaves it at $z = 1$. Finally, the unperturbed temperature profile is fixed by setting $T_0(z = 0.5) = 4.8$.

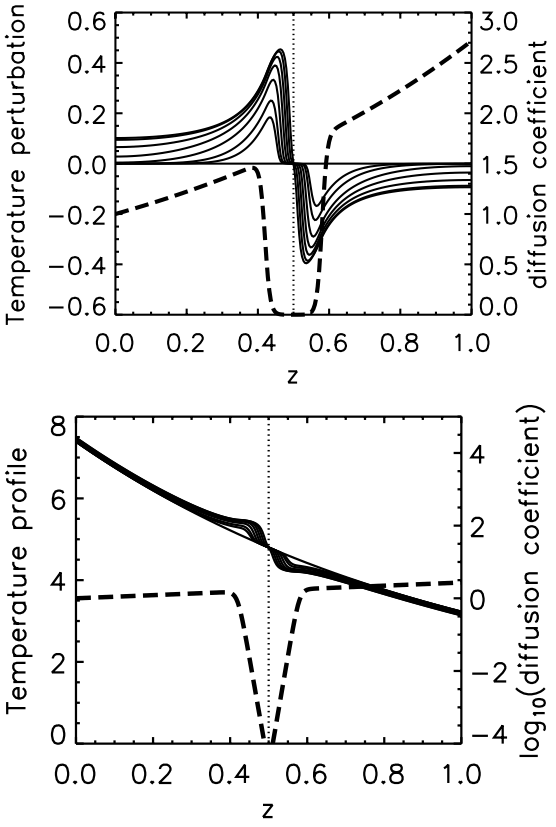

Fig. 2. Time evolution of the temperature profile starting from an unperturbed exponential profile after inclusion at time $t = 0$ of a partially conducting cylindrical domain around the center of the box. Upper panel: successive profiles of the temperature *perturbation* with increasingly higher maxima for increasing times. Lower panel: the full temperature profile. Superimposed on the figures (thick dashed line) is the profile of the thermal diffusivity $\tilde{\chi}(x = 0.5, z)$ (upper panel) and its logarithm (lower panel).

For the simulations we have taken the conductivity $\tilde{\kappa}(x,z)$ as the product of the inhomogeneous exponential profile of the unperturbed problem, $\kappa(z)$, times a *hole profile* as follows:

$$\tilde{\kappa}(x,z) = \kappa(z)\, h(x,z) \quad (36)$$

with $h(x,z)$ given by:

$$h(x,z) = \frac{1 + \tanh\left[\, \xi\, (r - W)\, \right]}{2}, \quad (37)$$

where r is the distance to the center of the tube, and W and ξ are parameters which define the width of the hole

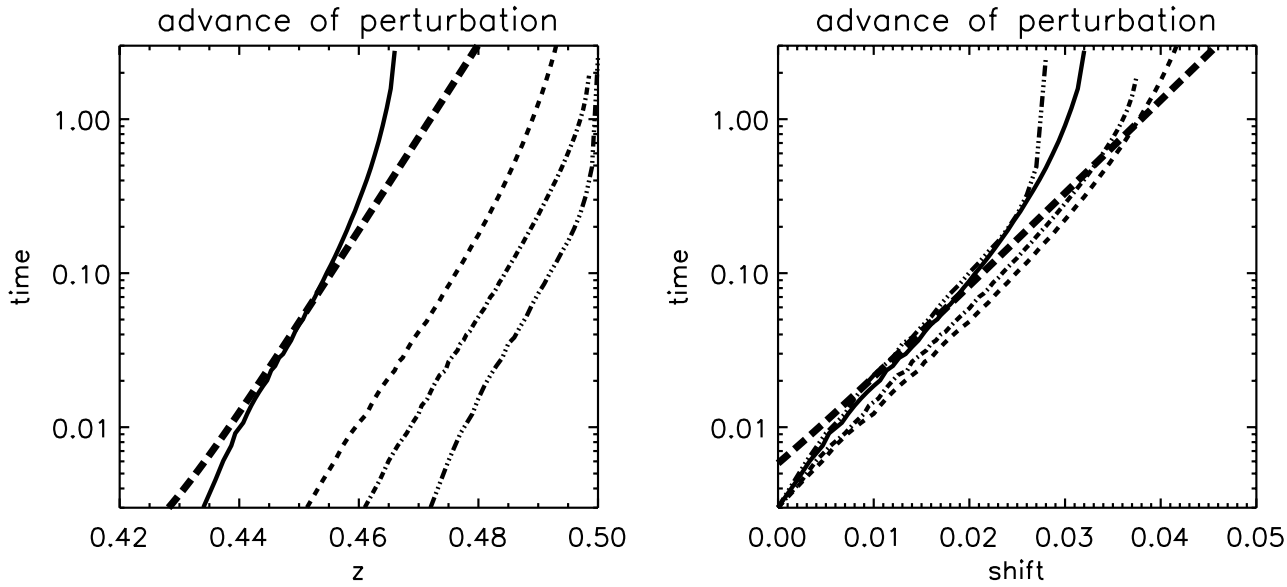

Fig. 3. Penetration of the perturbation into the cylinder: timescales. Left panel: the solid, short-dashed, dash-dotted and dash-triple dotted curves show the advance into the center of the tube of the position where the temperature perturbation is maximum, half-maximum, one tenth and one hundredth of the maximum, respectively. On the right panel, the same curves are shown but with the positions measured from the initial point of the corresponding curve on the left panel. The theoretical timescale $\tau = (R/z_{0,1})^2/\tilde{\chi}(x,z)$ is shown as a quasi-diagonal thick, dashed line.

and the steepness of its walls. A cut along $x = 0.5$ of the profile chosen in this section for $\tilde{\chi}(x,z) = \tilde{\kappa}(x,z)/c_{\rm p}$ is shown in Fig. 2 as a thick dashed line. The diameter of the isolating region has been taken $W = 0.08$. We use $\xi W = 5.6$, so that the function $h(x,z)$ tends to the value $\exp[2\xi(r-W)]$ in the neighborhood of the tube center and the conductivity is suppressed there by several orders of magnitude compared with its value outside.

In Fig. 2, the time evolution of the temperature profile along the symmetry axis $x = 0.5$ is shown for a number of successive instants. In the upper panel, the temperature *perturbation* is plotted, whereas on the lower panel the actual temperature profile is shown. The reduced conductivity in the tube causes a build-up of the temperature in front of the tube and a cool region (a thermal shadow) behind it. As time advances, the maximum and minimum of the perturbation grow in absolute value until an equilibrium is asymptotically reached. The local temperature maximum and minimum also serve to deviate the heat flow around the sides of the tube. The temperature profile close to the tube center stays almost unchanged for an extended time after the beginning of the calculation: the characteristic timescale for the evolution of the perturbation at a given position in the tube is $\tau = (R/z_{0,1})^2/\tilde{\chi}(x,z)$, with $z_{0,1}$ being the first zero of the Bessel function J_0 (see Sect. 4). This value becomes larger (in fact by several orders of magnitude) the closer to the tube center. As a result, the temperature profile is only gradually modified in the interior: the change in the temperature, as it were, *advances* into the tube only as far as the local diffusive timescale would allow it to.

This can be seen in more detail from Fig. 3. On the left panel (solid line) we have plotted in abscissas the position of the maximum of the temperature perturbation with time as ordinates. Three further curves on the diagram (short-dashed, dash-dotted and dash-triple dot) show the positions along the z-axis of the point in the temperature profile where the perturbation is 1/2, 1/10 and 1/100 of the maximum, respectively (from the two sides around the maximum, we choose the one closest to the box center). Finally, the theoretical timescale $\tau = (R/z_{0,1})^2/\tilde{\chi}(x = 0.5, z)$ is superimposed as a thick dashed quasi-diagonal line. We see that all curves are essentially parallel to the theoretical timescale all along the successive orders of magnitude in time (and, in fact, the curve for the maximum of the profile is quite close in value to it). Important deviations occur basically only when the final equilibrium position is approached (e.g., $z \to 0.5$ for the point with 1/100 the maximum temperature perturbation). This can also be seen on the right-hand side panel, where the positions are now plotted as *shift* from the initial position shown for each curve on the left panel.

The temperature perturbation visible in Fig. 2 is sufficient to divert essentially the whole heat flow around the diffusivity hole. This can be seen in Fig. 4, where the z- and x-components of the heat flow vector corresponding to the final stationary state are shown along four cuts in the box parallel to the z-axis, namely one along the symmetry axis $x = 0.5$ (solid), one (long-dashed) along the line $x = 0.57$, which cuts the cylinder close to its boundary, and two further cuts outside the cylinder ($x = 0.66$ and $x = 0.76$, drawn short dashed and dashed-dotted, respectively). The unperturbed value of the flow has been added in the upper panel as a thin solid horizontal line. Along the $x = 0.5$-line the z-component of the heat flow is completely suppressed in the interior of

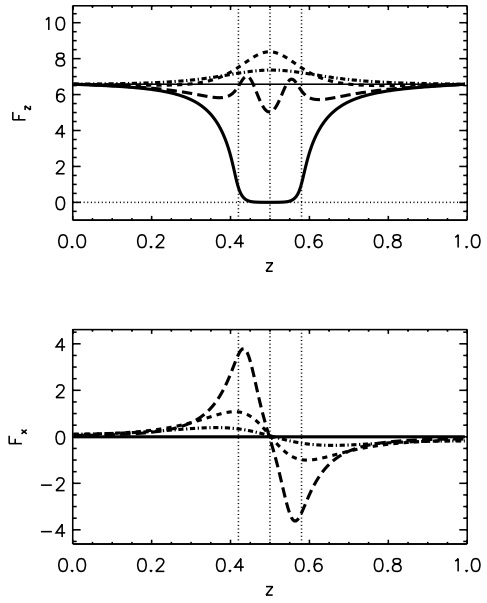

Fig. 4. z- and x-components of the heat flow along four cuts in the z-direction (solid: $x = 0.5$, i.e., the symmetry axis; long-dashed: $x = 0.57$; short-dashed: $x = 0.66$; dash-dotted: $x = 0.76$), The unperturbed value of the z-component is also shown as a thin solid line.

the tube; the x-component is zero there anyway by symmetry. Outside the cylinder and at the height where it is located, the F_z component is enhanced with respect to the unperturbed value (see the short-dashed), in order for the total flow across each horizontal cut to remain constant. This enhancement is still visible in the outskirts of the box ($x = 0.76$, dash-dotted curve). The x-component becomes fairly large in the periphery of the tube (long-dashed curve in the lower panel), to about two thirds of the z-component. $|F_x|$ becomes small as one moves further away from the tube (short-dashed and dash-dotted curves in the lower panel).

The stationary solution obtained in this section cannot be compared directly with the analytical solutions of the previous section since the internal thermal conductivity does not have an exponential profile as in Eq. (11), but is, rather, just a hole with a flat bottom and steep walls (even if the latter are smooth, to guarantee good numerical behavior). However, we can calculate the various terms in Eqs. (27) and (29) for the values used in the numerical solution. They are as follows:

$$\Delta T \;=\; 0.048, \tag{38}$$

$$a \;=\; 0.04, \tag{39}$$

$$QR \;=\; -\,\Delta T, \tag{40}$$

$$PR^2 \;=\; a\,\Delta T. \tag{41}$$

It follows that the stationary profile obtained in this section is essentially due to the pure thermal shadow terms in (27) and (29). As we will see in the following sections, this behavior is more adequate for isolating tubes in a purely radiative environment: in the solar convection zone (even in the overshoot region) we expect the convection to be sufficiently effective that a tiny temperature perturbation in front of and behind the tube can divert the whole heat flow around its periphery, so that the thermal shadow terms become much smaller than the P- and Q-terms.

4. Thin flux tube approximation

We have seen in Sect. 2 that the perturbation of the external temperature field is in the order of $\Delta T = F_0 R/\kappa_0$. Because of the high efficiency of convective energy transport, near the bottom of the solar convection zone we have $\Delta T \simeq 0.025\,\mathrm{K}$. The much larger temperature perturbation in the tube interior in the order of 100 K is mainly due to the curvature of the temperature profile and the spatial variation of the radiative conductivity (see Sect. 5). We may therefore assume that the temperature on the surface of the cylinder is a fixed function of height, so that we can derive the heating rate and the equilibrium temperature in the framework of the thin flux tube approximation (Roberts & Webb 1978; Spruit 1981; Ferriz-Mas et al. 1989) and compare them with the result of Sect. 2 as well as with the heating term derived by FF96.

Consider a parabolic profile of the external temperature (see Eq. (25)),

$$T_\mathrm{e}(z) = T_{\mathrm{e}0} + Qz + Pz^2\,, \tag{42}$$

and a linear function for the thermal conductivity within the cylinder,

$$\kappa_\mathrm{i}(z) = \kappa_{\mathrm{i}0}(1 + M_\mathrm{i} z)\,. \tag{43}$$

It turns out that only the first derivative of κ_i is relevant for the thin-tube result up to second order in the radial expansion, so we need not go to higher orders of z in (43). In polar coordinates we have

$$\kappa_\mathrm{i}(r,\phi) = \kappa_{\mathrm{i}0}(1 + M_\mathrm{i} r\cos\phi) \stackrel{\mathrm{def}}{=} \kappa_{\mathrm{i}0} + r\kappa_{i1}\,. \tag{44}$$

Together with the radial expansion of the (time-dependent) temperature field within the cylinder,

$$T_\mathrm{i}(r,\phi,t) = T_{\mathrm{i}0}(t) + rT_{i1}(\phi,t) + r^2 T_{i2}(\phi,t) + \ldots\,, \tag{45}$$

we insert Eq. (44) into the expression for the heating rate,

$$\mathcal{H} = \nabla\cdot(\kappa_\mathrm{i}\nabla T_\mathrm{i}) \;=\; \kappa_\mathrm{i}\Delta T_\mathrm{i} + (\nabla\kappa_\mathrm{i})\cdot(\nabla T_\mathrm{i})\,. \tag{46}$$

For the zeroth order, i.e. the heating rate at the tube center, we obtain

$$\mathcal{H}_0 = \kappa_{\mathrm{i}0}\left(\frac{T''_{i1}}{r} + \frac{T_{i1}}{r} + T''_{i2} + 4T_{i2}\right) + \kappa_{i1}T_{i1} + \kappa'_{i1}T'_{i1} \tag{47}$$

where primes indicate derivatives with respect to ϕ. The terms proportional to r^{-1} diverge for $r \to 0$ unless $T''_{i1} + T_{i1} = 0$, so that we have

$$T_{i1} = \tau_1\cos\phi \tag{48}$$

where τ_1 is determined by matching the solution to the external temperature at $r = R$. We have already omitted a term proportional to $\sin\phi$ since its coefficient becomes zero upon application of this boundary condition. Inserting Eq. (48) into Eq. (47) we find

$$\mathcal{H}_0 = \kappa_{\mathrm{i}0}(T''_{i2} + 4T_{i2} + M_\mathrm{i}\tau_1)\,. \tag{49}$$

Derivation of this equation with respect to ϕ yields

$$(T''_{i2} + 4T_{i2})' = 0\,, \tag{50}$$

so that

$$T_{i2} = \tau_2 \cos(2\phi) + \alpha(t)\,, \tag{51}$$

where we again have already omitted a term proportional to $\sin(2\phi)$ that vanishes upon application of the boundary condition. The three quantities, τ_1, τ_2, and α, are determined by matching the interior solution,

$$T_{\rm i}(r,\phi,t) = T_{\rm i0}(t) + r^2\alpha(t) + r\tau_1\cos\phi + r^2\tau_2\cos(2\phi) \tag{52}$$

to the external temperature at $r = R$

$$T_{\rm e}(R,\phi) = T_{\rm e0} + \frac{PR^2}{2} + RQ\cos\phi + R^2\frac{P}{2}\cos(2\phi)\,, \tag{53}$$

so that we obtain

$$\tau_1 = Q, \tag{54}$$

$$\tau_2 = \frac{P}{2}, \tag{55}$$

$$\alpha = \frac{T_{\rm e0} - T_{\rm i0}}{R^2} + \frac{P}{2}. \tag{56}$$

Consequently, we find for the heating rate

$$\mathcal{H}_0 = \frac{T_{\rm e0} - T_{\rm i0}}{R^2/4\kappa_{\rm i0}} + \kappa_{\rm i0}(2P + M_{\rm i}Q). \tag{57}$$

The first term on the right hand side of this equation represents the simple radiative heat exchange term (Moreno-Insertis 1983); the corresponding time scale, $c_{\rm p}R^2/(4\kappa_{\rm i0})$, agrees to within 30% with the exact solution for the lowest decay mode, $c_{\rm p}R^2/(z_{0,1}^2\kappa_{\rm i0})$, where $z_{0,1} \simeq 2.4$ is the first zero of the Bessel function J_0. The deviation of the thin-tube result from the exact solution even in the limit $R \to 0$ is caused by the fact that the second-order thin flux tube approximation forces the eigenfunction to stay parabolic out to $r = R$ (Ferriz-Mas et al. 1989). The second term on the r.h.s. of Eq. (57) agrees with the heating rate derived by FF96, namely the term $\nabla\cdot(\kappa\nabla T_{\rm e})$ taken at $r = 0$ ($z = 0$).

We obtain the equilibrium temperature at the tube center by setting $\mathcal{H}_0 = 0$ in Eq. (57). The result is

$$T_{\rm i0} = T_{\rm e0} + \frac{R^2}{4}(2P + M_{\rm i}Q) \stackrel{\rm def}{=} T_{\rm eq,0} \tag{58}$$

and, using Eq. (52), the equilibrium solution in the whole cylinder becomes

$$T_{\rm eq}(r,\phi) = T_{\rm e0} + \frac{PR^2}{2} + \frac{M_{\rm i}Q}{4}(R^2 - r^2) + rQ\cos\phi + \frac{Pr^2}{2}\cos(2\phi)\,. \tag{59}$$

The corresponding temperature perturbation with respect to the background profile,

$$T_{\rm eq}(r,\phi) - T_{\rm e}(r,\phi) = \left(\frac{PR^2}{2} + \frac{M_{\rm i}QR^2}{4}\right)\left(1 - \frac{r^2}{R^2}\right), \tag{60}$$

agrees with the solution given in Eq. (27) in the limit of negligible thermal shadow effects ($\Delta T \to 0$).

In the framework of the thin flux tube approximation, it is easy to estimate how strongly the perturbation of the radiative conductivity caused by the temperature perturbation affects the equilibrium temperature and the heating rate. We replace Eq. (43) by

$$\kappa_{\rm i}(z) = \kappa_{\rm i0}(1 + M_{\rm i}z) + \delta\kappa(z)\,. \tag{61}$$

and write the perturbation of the radiative conductivity as

$$\frac{\delta\kappa}{\kappa_{\rm i0}} = 8.5\frac{T_{\rm i} - T_{\rm e}(z)}{T_{\rm e0}}\,, \tag{62}$$

assuming Kramer's opacity law, $\kappa \propto T^{6.5}\rho^{-2}$ and $\delta\rho/\rho = -\delta T/T$ for a thin flux tube with $\beta \gg 1$. Repeating the same steps as in Eqs. (44–58) leads to the equilibrium temperature perturbation at the tube center, viz.

$$T_{\rm eq,0} - T_{\rm e0} = \frac{R^2}{4}(2P + M_{\rm i}Q)\left(1 + \frac{8.5M_{\rm i}QR^2}{4T_{\rm e0}}\right)\cdot \tag{63}$$

Inserting values corresponding to the conditions in the lower solar convection zone (see Sect. 5) and a tube radius of 1000 km, we find that the relative difference to the result with no κ perturbation given in Eq. (58) is a few times 10^{-4} and therefore negligible.

5. Magnetic flux tubes in the solar convection zone

In order to evaluate the consequences of the thermal energy exchange for magnetic flux storage in the solar interior, we consider flux tubes in the lower convection zone and in the overshoot layer. From the convection zone model of Spruit (1977a) we derive the following values for the various quantities that are relevant in our context:

$$\kappa_0 = 5\times10^{20}\,\mathrm{erg\ (cm\ s\ K)^{-1}}\,,$$

$$\kappa_{\rm i0} = 8.1\times10^{14}\,\mathrm{erg\ (cm\ s\ K)^{-1}}\,,$$

$$\kappa_{\rm i0}/\kappa_0 = 1.6\times10^{-6}\,,$$

$$T_{\rm e0} = 2.2\times10^{6}\,\mathrm{K}\,,$$

$$M = 10^{-9}\,\mathrm{cm^{-1}}\,,$$

$$M_{\rm i} = -2.5\times10^{-10}\,\mathrm{cm^{-1}}\,,$$

$$Q = -1.6\times10^{-4}\,\mathrm{K\ cm^{-1}}\,,$$

$$P = 3\times10^{-15}\,\mathrm{K\ cm^{-2}}\,. \tag{64}$$

These values apply to the bottom of the convection zone proper as well as to the overshoot region. The value for M cannot be determined very precisely from the convection zone model; our estimate gives the order of magnitude of that quantity in the lowermost 15 Mm of the convection zone. For $M_{\rm i}$ we have used Kramer's law (see Eq. (17)

of FF96). The quantity Q essentially represents the adiabatic temperature gradient while P (proportional to the second derivative of T_0) is determined from

$$\frac{\mathrm{d}^2 T_0}{\mathrm{d}z^2} = -\frac{\mathrm{d}}{\mathrm{d}z}\left(\frac{T_0 \nabla}{H_\mathrm{p}}\right) = -\frac{\nabla \bar{\mu}}{\mathcal{R}}\left(\frac{\mathrm{d}g}{\mathrm{d}z}\right) - \frac{\bar{\mu} g}{\mathcal{R}}\left(\frac{\mathrm{d}\nabla}{\mathrm{d}z}\right), \quad (65)$$

where ∇ is the logarithmic temperature gradient, H_p the pressure scale height, $\bar{\mu}$ the mean molecular weight (assumed to be constant), $\mathcal{R}$ the gas constant, and g the gravitational acceleration. Inserting values, it turns out that the second term on the r.h.s. of Eq. (65) is two orders of magnitude smaller than the first term. The correction due to the spherical geometry ($F_0 \propto r^{-2}$ in spherical coordinates) is even four orders of magnitude smaller than the first term. Consequently, the value of P near the bottom of the solar convection zone is practically only determined by the outward decrease of the gravitational acceleration; in particular, it is independent of the specific description of the convective energy transport as long as the stratification is nearly adiabatic. Clearly, the same statement is true for the temperature gradient, Q.

For a quantitative estimate we consider a magnetic flux tube with a radius of $R = 1000$ km radius and a field strength of $B = 10^5$ G. The tube contains a magnetic flux of $\Phi_\mathrm{mag} \simeq 3 \times 10^{21}$ Mx, which is a typical value for a sunspot. Such tubes are thought to be stored in the convective overshoot layer prior to their eruption to form sunspot groups and magnetically active regions (e.g. Moreno-Insertis et al. 1992; Caligari et al. 1995). The values of the R-dependent quantities are then

$$a = \frac{MR}{2} \;=\; 5 \times 10^{-2}\,,$$

$$a_\mathrm{i} = \frac{M_\mathrm{i} R}{2} \;=\; -1.3 \times 10^{-2}\,,$$

$$\Delta T = \frac{F_0 R}{\kappa_0} = 2.5 \times 10^{-2}\,\mathrm{K}\,,$$

$$\eta = -[0.577 + \ln(a/2)]^{-1} \;=\; 0.32. \quad (66)$$

Since $\kappa_{\mathrm{i}0} \ll \kappa_0$, we can use Eq. (27) for the temperature perturbation within the flux tube. The excess temperature (with respect to the background stratification) at the tube center ($r = 0$), ΔT_eq, can then be written as a sum of contributions arising from different physical effects:

$$\Delta T_\mathrm{eq} \stackrel{\mathrm{def}}{=} T_\mathrm{i}'(r=0) = \Delta T_\mathrm{S} + \Delta T_\mathrm{P} + \Delta T_\kappa\,, \quad (67)$$

where

$$\Delta T_\mathrm{S} = \left[a\left(\frac{1}{2} - \gamma - \ln\frac{a}{2}\right) - \frac{a_\mathrm{i}}{2}\right] \Delta T \;\simeq\; 10^{-4}\,\mathrm{K} \quad (68)$$

represents the effect of the perturbation of the external temperature field (thermal shadow). The smallness of ΔT_S shows that thermal shadow effects are negligible in the case considered here; this is due to the large value of κ_0. The other two terms in Eq. (67) describe the contribution due to the curvature of the background temperature,

$$\Delta T_\mathrm{P} = \frac{P R^2}{2} \simeq 15\,\mathrm{K}\,, \quad (69)$$

and the contribution resulting from the spatial variation of the radiative thermal conductivity,

$$\Delta T_\kappa = \frac{a_\mathrm{i} Q R}{2} \simeq 100\,\mathrm{K}\,. \quad (70)$$

Therefore, the net temperature excess of

$$\Delta T_\mathrm{eq} \simeq 115 \cdot (R/1000\,\mathrm{km})^2\,\mathrm{K} \quad (71)$$

is primarily determined by the divergence of the background radiative heat flux (as suggested by FF96, see also Sect. 4 above), which, in turn, is dominated by the outward decrease of the radiative conductivity.

Comparing ΔT_eq with the temperature deficit corresponding to neutral buoyancy of a (thin) flux tube, $\Delta T_\mathrm{B} = T_{\mathrm{e}0}/\beta \simeq 13\,\mathrm{K}$ (with $B = 10^5$ G, $\beta \simeq 1.6 \times 10^5$), with the variation of the background temperature over the diameter of a horizontal tube, $\Delta T_\mathrm{D} = 2R\,|Q| \simeq 3.2 \times 10^4\,\mathrm{K}$, and with the variation of potential temperature, $\Delta T_\delta = 2R\,|\delta| T/H_\mathrm{p} \simeq 0.1\,\mathrm{K}$ (for $|\delta| = |\nabla - \nabla_\mathrm{ad}| \simeq 10^{-6}$), we find the scaling

$$\Delta T_\delta \ll \Delta T_\mathrm{B} < \Delta T_\mathrm{eq} \ll \Delta T_\mathrm{D}. \quad (72)$$

The ratio of ΔT_eq and ΔT_B is

$$\frac{\Delta T_\mathrm{eq}}{\Delta T_\mathrm{B}} = \frac{2\Phi_\mathrm{mag}\, p_{\mathrm{e}0}\,(2P + M_\mathrm{i} Q)}{B^3\, T_{\mathrm{e}0}}$$

$$\simeq 8.8\left(\frac{\Phi_\mathrm{mag}}{3 \times 10^{21}\,\mathrm{Mx}}\right)\left(\frac{B}{10^5\,\mathrm{G}}\right)^{-3}, \quad (73)$$

where Φ_mag is the magnetic flux of the tube and $p_{\mathrm{e}0}$ is the external pressure at $z = 0$, the height of the tube center. Whenever this ratio is of order one or larger, the heating effect due to the variation of the radiative energy flux leads to a significant buoyancy of the tube and therefore must be taken into account in studies of magnetic flux storage and evolution. Consequently, radiative heating cannot be ignored for the kind of flux tubes that are thought to be the sources for the emerging active regions at the solar surface. We can see this also by considering the time evolution of the internal temperature in the thin flux tube approximation (cf. Sect. 4). In the simplest case we have

$$\frac{\mathrm{d}T_{\mathrm{i}0}(t)}{\mathrm{d}t} = \frac{T_\mathrm{eq} - T_{\mathrm{i}0}(t)}{\tau_0} \quad (74)$$

with

$$\tau_0 = \frac{0.17 R^2 c_\mathrm{p}}{\kappa_{\mathrm{i}0}} \simeq 5.4\,\mathrm{yr} \quad (75)$$

in the case of our "standard" flux tube of 1000 km radius. How long does it take for an initially neutrally buoyant tube with

$$T_{\mathrm{i}0}(0) = T_{\mathrm{e}0}(1 - \beta^{-1}) = T_{\mathrm{e}0} - \Delta T_\mathrm{B} \quad (76)$$

to reach the temperature $T_{\mathrm{e}0}$ and so acquire a significant buoyancy force? Writing $T_{\mathrm{i}0}(t_\mathrm{B}) = T_{\mathrm{e}0}$, we find

$$t_\mathrm{B} = \tau_0\, \ln\left(1 + \frac{\Delta T_\mathrm{B}}{\Delta T_\mathrm{eq}}\right). \quad (77)$$

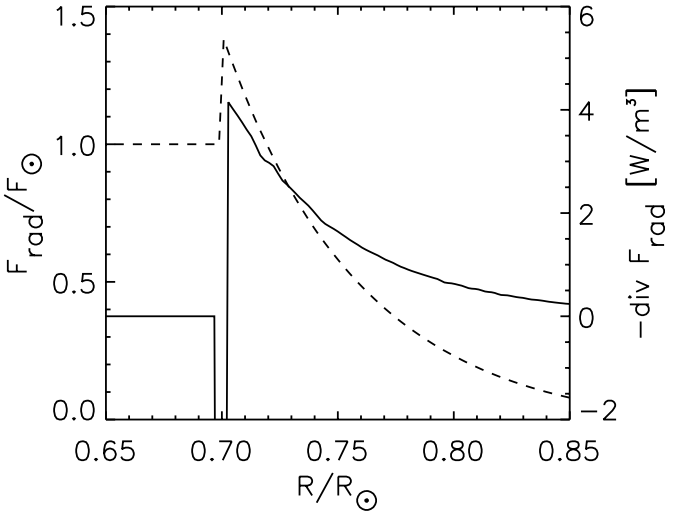

Fig. 5. Radiative energy flux in units of the total solar flux (dotted line) and volume heating rate (full line) as a function of radius for a model of the solar convection zone with overshoot (Skaley & Stix 1991).

As long as $\epsilon = \Delta T_{\rm B}/\Delta T_{\rm eq}$ remains sufficiently small, so that we can write $\ln(1+\epsilon) \simeq \epsilon$, $t_{\rm B}$ becomes independent of the tube radius:

$$t_{\rm B} \simeq \frac{0.68 c_{\rm p} T_{\rm e0}}{\beta(2P + M_{\rm i} Q)\kappa_{\rm i0}} \simeq 0.6\,{\rm yr}\,. \tag{78}$$

Consequently, flux tubes stored near the bottom of the convection zone become significantly buoyant within less than a year. This raises questions with regard to flux storage in the convective overshoot region. As discussed in a subsequent paper (Rempel et al. 2002), storage times comparable to the length of the solar cycle require a rather strongly subadiabatic stratification with $\delta \lesssim -10^{-4}$ if the radiative heating effect is included.

Figure 5 gives the undisturbed radiative energy flux in units of the total solar flux (dashed line) and the volume heating rate $-\nabla \cdot \boldsymbol{F}_{\rm rad} = \nabla \cdot (\kappa \nabla T)$ (thick line) as a function of the radius for a model of the solar convection zone with overshoot (Skaley & Stix 1991). The overshoot layer corresponds to the region where the convective energy flux is directed inward, so that $F_{\rm rad}/F_\odot > 1$. Apart from a thin boundary layer of thickness $\lesssim$1000 km at the transition to the radiative core, the radiative flux decreases outward, so that the heating rate is positive over the bulk of the overshoot layer and in the lower convection zone. A typical value in the overshoot layer is 3 W m^{-3}.

6. Summary and discussion

In order to study the thermal properties of magnetic flux tubes embedded in a non-magnetic fluid, we have studied a general two-dimensional thermal diffusion problem. Both the flux tube and its exterior have been considered, allowing for inhomogeneous heat conductivities in both regions. The case of small tube radius in comparison to the scales over which the diffusivities vary admits an analytical solution.

The case of a flux tube embedded in a convective region with internally suppressed convective energy transport can be treated within the framework of this model by (a) using the diffusion approximation for the radiative energy transport inside and outside the tube and (b) applying to the perturbation in the convective transport, caused by the presence of the tube the linear approximation of Spruit (1977a), so that it can be treated as a diffusion process as well. Under the conditions of the lower solar convection zone, the external temperature perturbation is almost negligible, owing to the very large efficiency of the convective energy transport in diverting the blocked convective heat flow around the tube. Significant thermal shadows and hot spots can emerge only in the case of thermal *blankets* blocking the convection over a horizontally extended region (Parker 1987).

When the external temperature perturbation is negligible, the internal thermal structure of the tube interior is determined by the undisturbed external temperature stratification, in particular by the curvature of the temperature profile (the coefficient P in Eq. (25)) and by the spatial variation of the radiative heat conductivity. Both quantities are independent of the detailed model of convective energy transport as long as the stratification is nearly adiabatic. The thermal effect of the external temperature profile near the bottom of the solar convection zone corresponds to a radiative heating of the flux tube equal in amount to the negative divergence of the external radiative heat flow, in accordance with the result of FF96. The same result is found by using a thin flux tube approximation to the second order in a tube radius with a fixed external temperature profile.

While the thermal equilibrium resulting within the tube can be well understood using the (analytical) tools developed and explained in this paper, the question of how this equilibrium can be reached cannot be answered in a simple or unique way. Whenever the dynamics can be disregarded and the simple assumption of constant pressure and zero velocity can be sustained, one can solve the time dependent problem as a purely diffusive phenomenon with inhomogeneous diffusivity coefficients. With the help of the simple example treated in Sect. 3 by means of a computer code, one can understand that the establishment of the thermal equilibrium in and around a strongly insulating tube proceeds gradually, the equilibrium profile being established at each point on the timescale provided by the *local* value of the diffusivity. This means that the perturbation *advances* into the less diffusive regions on a (much) slower timescale than in the rest of the integration domain. This is at variance with the simple image that lies at the base of the thin flux tube approximation (at least, of its zero-order version).

Consideration of the dynamics ensuing from the thermal evolution adds a new dimension (and a large degree of complication) to the problem. As shown by Lenz et al. (2002), long before the establishment of the thermal

equilibrium solution the density differences arising within the tube cross-section through the thermal processes cause a dynamical evolution which leads to the loss of the simple tube-like structure. The detailed evolution (and the degree of loss of the simple tube-like shape) depend on the initial conditions, e.g., whether the magnetic field is twisted in the tube or otherwise. Hence, there is no unique answer to the time evolution problem.

In the simple case that the tube-like shape is conserved, the effects discussed in this paper are relevant for the problem of the storage of the magnetic field in the lower convection zone of the Sun. As shown in a forthcoming paper (Rempel et al. 2002), the heating of the tube caused by the non-zero divergence of the radiative flux makes the tubes rise from their original position of storage in the overshoot region to the main bulk of the convection zone (and from there to the photosphere) on a timescale which, for the case of tubes with field strength 10^5 G and radius of 1000 km, is short compared with the solar activity cycle period. If this fate were to be avoided, the logarithmic temperature gradient in the overshoot region should be below adiabatic by an amount of at least $\delta \simeq -10^{-4}$ (which, in fact, may not be unrealistic: see Xiong & Deng 2001).

The general formalism developed in this paper is well applicable to magnetic structures in the radiative core of the Sun, where the radiative heat conductivity is affected by temperature perturbations (e.g. those developing in a neutrally buoyant flux tube). As pointed out by Parker (1984a,b), thermal shadows in this case could lead to circulation flows and lithium mixing. We shall consider this problem in subsequent work.

Acknowledgements. Financiation through DGES project PB95-0028C of the Spanish Ministry of Education is acknowledged. We are grateful to Dr. M. Rempel for helpful discussions and for providing Fig. 5.

Appendix A: Solution for small cylinder radius

In order to determine an approximate solution of Eqs. (14) and (15) in the limit $|a| \ll 1$ and $|a_i| \ll 1$, we expand the matching conditions, Eqs. (20) and (23), in powers of a and a_i up to second order and truncate the Fourier series at $m = 2$. Using Eq. (26) for the background temperature, we obtain from Eq. (20):

$$\begin{aligned}
&\left(T_{\rm e0} + a^2\frac{2P}{M^2}\right) + 2a\frac{Q}{M}\cos\phi + a^2\frac{2P}{M^2}\cos(2\phi) \\
&\quad + \left[\left(1+\frac{a^2}{4}\right) - a\cos\phi + \frac{a^2}{4}\cos(2\phi)\right] \\
&\quad \times \left[G_0 + G_1\cos\phi + G_2\cos(2\phi)\right] \\
&= \left[\left(1+\frac{a_{\rm i}^2}{4}\right) - a_{\rm i}\cos\phi + \frac{a_{\rm i}^2}{4}\cos(2\phi)\right] \\
&\quad \times \left[H_0 + H_1\cos\phi + H_2\cos(2\phi)\right]. \qquad \text{(A.1)}
\end{aligned}$$

The matching condition for the normal component of the heat flux, Eq. (23), yields:

$$\begin{aligned}
&2a\delta T\cos\phi + \left[\left(1+\frac{a^2}{4}\right) + a\cos\phi + \frac{a^2}{4}\cos(2\phi)\right] \\
&\quad \times \left[G_0\left(a\cos\phi + a\frac{\mathcal{K}_1(a)}{\mathcal{K}_0(a)}\right)\right. \\
&\quad + G_1\left(a\cos\phi - 1 + a\frac{\mathcal{K}_2(a)}{\mathcal{K}_1(a)}\right)\cos\phi \\
&\quad \left. + G_2\left(a\cos\phi - 2 + a\frac{\mathcal{K}_3(a)}{\mathcal{K}_2(a)}\right)\cos(2\phi)\right] \\
&= \frac{\kappa_{\rm i0}}{\kappa_0}\left[\left(1+\frac{a_{\rm i}^2}{4}\right) + a_{\rm i}\cos\phi + \frac{a_{\rm i}^2}{4}\cos(2\phi)\right] \\
&\quad \times \left[H_0\left(a_{\rm i}\cos\phi - a_{\rm i}\frac{\mathcal{I}_1(a_{\rm i})}{\mathcal{I}_0(a_{\rm i})}\right)\right. \\
&\quad + H_1\left(a_{\rm i}\cos\phi - 1 - a_{\rm i}\frac{\mathcal{I}_2(a_{\rm i})}{\mathcal{I}_1(a_{\rm i})}\right)\cos\phi \\
&\quad \left. + H_2\left(a_{\rm i}\cos\phi - 2 - a_{\rm i}\frac{\mathcal{I}_3(a_{\rm i})}{\mathcal{I}_2(a_{\rm i})}\right)\cos(2\phi)\right]. \qquad \text{(A.2)}
\end{aligned}$$

We use the approximations (cf. Abramowitz & Stegun 1965; Ch. 9.6)

$$a_{\rm i}\frac{\mathcal{I}_1(a_{\rm i})}{\mathcal{I}_0(a_{\rm i})} = \frac{a_{\rm i}^2}{2} + \mathcal{O}({a_{\rm i}}^4) \qquad \text{(A.3)}$$

$$a_{\rm i}\frac{\mathcal{I}_2(a_{\rm i})}{\mathcal{I}_1(a_{\rm i})} = \frac{a_{\rm i}^2}{4} + \mathcal{O}({a_{\rm i}}^4) \qquad \text{(A.4)}$$

$$a_{\rm i}\frac{\mathcal{I}_3(a_{\rm i})}{\mathcal{I}_2(a_{\rm i})} = \frac{a_{\rm i}^2}{6} + \mathcal{O}({a_{\rm i}}^4) \qquad \text{(A.5)}$$

$$a_{\rm i}\frac{\mathcal{K}_2(a)}{\mathcal{K}_1(a)} = 2 + \mathcal{O}(a^2) \qquad \text{(A.6)}$$

$$a_{\rm i}\frac{\mathcal{K}_3(a)}{\mathcal{K}_2(a)} = 4 + \mathcal{O}(a^4) \qquad \text{(A.7)}$$

$$a_{\rm i}\frac{\mathcal{K}_1(a)}{\mathcal{K}_0(a)} = \eta - \frac{a^2}{2}\left[1 + \frac{\eta}{2}(2+\eta)\right] + \mathcal{O}(a^4) \qquad \text{(A.8)}$$

with

$$\eta = -\left[\ln\left(\frac{a}{2}\right) + \gamma\right]^{-1}, \qquad \text{(A.9)}$$

$\gamma = 0.57721...$ (Euler's constant).

We equate the coefficients of the terms $\propto \cos(m\phi)$, $m = 0, 1, 2$, on both sides of Eqs. (A.1) and (A.2), respectively, and thus obtain six algebraic equations for the expansion coefficients, G_m and H_m, $m = 0, 1, 2$:

$$\begin{aligned}
&T_{\rm e0} + a^2\frac{2P}{M^2} + G_0\left(1+\frac{a^2}{4}\right) - G_1\frac{a}{2} \\
&\quad = H_0\left(1+\frac{a_{\rm i}^2}{4}\right) - H_1\frac{a_{\rm i}}{2} \qquad \text{(A.10)}
\end{aligned}$$

$$2a\frac{Q}{M} - G_0 a + G_1 = -H_0 a_\mathrm{i} + H_1 \tag{A.11}$$

$$a^2\frac{2P}{M^2} + G_0\frac{a^2}{4} - G_1\frac{a}{2} + G_2 = H_0\frac{a_\mathrm{i}^2}{4} - H_1\frac{a_\mathrm{i}}{2} + H_2 \tag{A.12}$$

$$G_0\eta\left[1 - \frac{a^2}{4}(1+\eta)\right] + G_1 a = 0 \tag{A.13}$$

$$2a\delta T + G_0 a(1+\eta) + G_1 = \frac{\kappa_{\mathrm{i}0}}{\kappa_0}\left(H_0 a_\mathrm{i} - H_1\right) \tag{A.14}$$

$$G_0\frac{a^2}{4}(2+\eta) + G_1 a + 2G_2 = \frac{\kappa_{\mathrm{i}0}}{\kappa_0}\left(H_0\frac{a_\mathrm{i}^2}{2} - 2H_2\right)\cdot \tag{A.15}$$

In deriving this set of equations we have assumed that $G_m, H_m \le \mathcal{O}(a^m, a_\mathrm{i}^m)$. This assumption can be justified either by solving the set of equations including the neglected terms or, a posteriori, by solving Eqs. (A.10)–(A.15) to first order in (a, a_i) and taking the limits $a \to 0$ and $a_\mathrm{i} \to 0$. We then find $H_0 = \mathcal{O}(a^0, a_\mathrm{i}^0)$, $(H_1, G_1) = \mathcal{O}(a^1, a_\mathrm{i}^1)$, and $(G_0, G_2, H_2) = \mathcal{O}(a^2, a_\mathrm{i}^2, aa_\mathrm{i})$. The weak (logarithmic) dependence of η on a does not affect these conclusions. This allows us to further simplify the set of equations by neglecting all terms proportional to $G_0 a$ and $G_0 a^2$. Furthermore, Eqs. (A.10), (A.11), (A.13), and (A.14), form an independent subset of equations for G_0, G_1, H_0, and H_1:

$$T_{\mathrm{e}0} + a^2\frac{2P}{M^2} + G_0 - G_1\frac{a}{2} = H_0\left(1 + \frac{a_\mathrm{i}^2}{4}\right) - H_1\frac{a_\mathrm{i}}{2} \tag{A.16}$$

$$2a\frac{Q}{M} + G_1 = -H_0 a_\mathrm{i} + H_1 \tag{A.17}$$

$$G_0\eta + G_1 a = 0 \tag{A.18}$$

$$2a\delta T + G_1 = \frac{\kappa_{\mathrm{i}0}}{\kappa_0}\left(H_0 a_\mathrm{i} - H_1\right)\cdot \tag{A.19}$$

To second order, the expansion coefficients resulting from this set of equations are:

$$G_0 = \frac{2a^2}{\eta}\frac{\kappa_0}{\kappa_0 + \kappa_{\mathrm{i}0}}\left(\frac{\kappa_{\mathrm{i}0}}{\kappa_0}\frac{Q}{M} + \delta T\right) \tag{A.20}$$

$$G_1 = -2a\frac{\kappa_0}{\kappa_0 + \kappa_{\mathrm{i}0}}\left(\frac{\kappa_{\mathrm{i}0}}{\kappa_0}\frac{Q}{M} + \delta T\right) \tag{A.21}$$

$$H_0 = T_{\mathrm{e}0}\left(1 + \frac{a_\mathrm{i}^2}{4}\right) + aa_\mathrm{i}\frac{\kappa_0}{\kappa_0 + \kappa_{\mathrm{i}0}}\left(\frac{Q}{M} - \delta T\right) + a^2\left[\frac{2P}{M^2} + \frac{\kappa_0}{\kappa_0 + \kappa_{\mathrm{i}0}}\left(\frac{2}{\eta} + 1\right)\left(\frac{\kappa_{\mathrm{i}0}}{\kappa_0}\frac{Q}{M} + \delta T\right)\right] \tag{A.22}$$

$$H_1 = a_\mathrm{i} T_{\mathrm{e}0} + 2a\frac{\kappa_0}{\kappa_0 + \kappa_{\mathrm{i}0}}\left(\frac{Q}{M} - \delta T\right)\cdot \tag{A.23}$$

The coefficients G_2 and H_2 follow by inserting these expressions into Eqs. (A.12) and (A.15), again omitting the fourth-order terms proportional to $G_0 a^2$:

$$G_2 = -aa_\mathrm{i}\frac{\kappa_{\mathrm{i}0}}{\kappa_0}\left(\frac{\kappa_0}{\kappa_0 + \kappa_{\mathrm{i}0}}\right)^2\left(\frac{Q}{M} - \delta T\right) - \frac{a^2\kappa_{\mathrm{i}0}}{\kappa_0 + \kappa_{\mathrm{i}0}} \times \left[\frac{2P}{M^2} + \frac{\kappa_0}{\kappa_{\mathrm{i}0}}\left(\frac{\kappa_{\mathrm{i}0} - \kappa_0}{\kappa_{\mathrm{i}0} + \kappa_0}\right)\left(\frac{\kappa_{\mathrm{i}0}}{\kappa_0}\frac{Q}{M} + \delta T\right)\right] \tag{A.24}$$

$$H_2 = \frac{T_{\mathrm{e}0}a_\mathrm{i}^2}{4} + aa_\mathrm{i}\left(\frac{\kappa_0}{\kappa_0 + \kappa_{\mathrm{i}0}}\right)^2\left(\frac{Q}{M} - \delta T\right) + 2a^2\frac{\kappa_0}{\kappa_0 + \kappa_{\mathrm{i}0}}\left[\frac{P}{M^2} + \frac{\kappa_0}{\kappa_0 + \kappa_{\mathrm{i}0}}\left(\frac{\kappa_{\mathrm{i}0}}{\kappa_0}\frac{Q}{M} + \delta T\right)\right]\cdot \tag{A.25}$$

General expressions for the external and internal temperature perturbations can be determined by expanding Eqs. (18) and (19) in Sect. 2 up to second order in a and a_i, truncating the expansion in azimuth angle at $m = 2$, and inserting the coefficients given by Eqs. (A.20)–(A.25). In the lower parts of the solar convection zone we can additionally take the limit $\kappa_{\mathrm{i}0} \ll \kappa_0$ and obtain to first order in $\kappa_{\mathrm{i}0}/\kappa_0$ the expressions

$$\begin{aligned} T_\mathrm{i}'(r,\phi) = {} & \frac{1}{2}\left[PR^2 + a_\mathrm{i}\left(1 - \frac{\kappa_{\mathrm{i}0}}{\kappa_0}\right)(QR - \Delta T)\right] \\ & \times\left(1 - \frac{r^2}{R^2}\right) + \left(\frac{\kappa_{\mathrm{i}0}}{\kappa_0}QR + \Delta T\right) \\ & \times\left[a\left(\frac{1}{2} - \ln\frac{MR}{4} - \gamma\right) - \frac{r}{R}\cos\phi\right] \\ & + \left\{a\left(\frac{\kappa_{\mathrm{i}0}}{\kappa_0}QR + \Delta T\right)\right. \\ & \left. - \frac{1}{2}\frac{\kappa_{\mathrm{i}0}}{\kappa_0}\left[PR^2 + a_\mathrm{i}(QR - \Delta T)\right]\right\}\frac{r^2}{R^2}\cos 2\phi \end{aligned} \tag{A.26}$$

$$\begin{aligned} T_\mathrm{e}'(r,\phi) = {} & a\left(\frac{\kappa_{\mathrm{i}0}}{\kappa_0}QR + \Delta T\right)\left(\frac{1}{2} - \ln\frac{Mr}{4} - \gamma\right) \\ & - \left(\frac{\kappa_{\mathrm{i}0}}{\kappa_0}QR + \Delta T\right)\frac{R}{r}\cos\phi \\ & + \frac{1}{2}\left\{a\left(\frac{\kappa_{\mathrm{i}0}}{\kappa_0}QR + \Delta T\right)\left(1 + \frac{r^2}{R^2}\right)\right. \\ & \left. - \frac{\kappa_{\mathrm{i}0}}{\kappa_0}\left[PR^2 + a_\mathrm{i}(QR - \Delta T)\right]\frac{R^2}{r^2}\right\}\cos 2\phi \end{aligned} \tag{A.27}$$

where $\Delta T = 2a\delta T$. If in the undisturbed state the radiative heat flux is much smaller than the convective flux, i.e. if $\kappa_\mathrm{i}|Q|R \ll \kappa_0\,\Delta T$, we can restrict ourselves to the zeroth order in $\kappa_\mathrm{i}/\kappa_0$ and obtain the expressions given by Eqs. (27) and (29) in Sect. 2.

References

Caligari, P., Moreno-Insertis, F., & Schüssler, M. 1995, ApJ, 441, 886

Caligari, P., Schuessler, M., & Moreno-Insertis, F. 1998, ApJ, 502, 481
Choudhuri, A. R., & Gilman, P. A. 1987, ApJ, 316, 788
D'Silva, S., & Choudhuri, A. R. 1993, A&A, 272, 621
Fan, Y., & Fisher, G. H. 1996, Sol. Phys., 166, 17
Fan, Y., Fisher, G. H., & McClymont, A. N. 1994, ApJ, 436, 907
Ferriz-Mas, A., Schüssler, M., & Anton, V. 1989, A&A, 210, 425
Lenz, D., Moreno-Insertis, F., & Schüssler, M. 2002, ApJ, in preparation
Moreno-Insertis, F. 1983, A&A, 122, 241
Moreno-Insertis, F. 1986, A&A, 166, 291
Moreno-Insertis, F. 1992, in NATO ASI Proc. 375: Sunspots. Theory and Observations (Dordrecht: Kluwer Academic Publishers), 385
Moreno-Insertis, F., Schüssler, M., & Ferriz-Mas, A. 1992, A&A, 264, 686
Parker, E. N. 1975, ApJ, 198, 205
Parker, E. N. 1984a, ApJ, 286, 677
Parker, E. N. 1984b, ApJ, 286, 666
Parker, E. N. 1987, ApJ, 321, 984
Rempel, M., Schüssler, M., & Moreno-Insertis, F. 2002, A&A, in preparation
Rempel, M., Schüssler, M., & Tóth, G. 2000, A&A, 363, 789
Roberts, B., & Webb, A. R. 1978, Sol. Phys., 56, 5
Schüssler, M. 1983, in Solar and Stellar Magnetic Fields: Origins and Coronal Effects (Dordrecht: Kluwer Academic Publishers), IAU Symp., 102, 213
Schüssler, M., Caligari, P., Ferriz-Mas, A., & Moreno-Insertis, F. 1994, A&A, 281, L69
Skaley, D., & Stix, M. 1991, A&A, 241, 227
Spruit, H. C. 1977a, Sol. Phys., 55, 3
Spruit, H. C. 1977b, Ph.D. Thesis, University of Utrecht, The Netherlands
Spruit, H. C. 1981, A&A, 102, 129
Spruit, H. C., & van Ballegooijen, A. A. 1982, A&A, 106, 58
Tobias, S. M., Brummell, N. H., Clune, T. L., & Toomre, J. 1998, ApJ, 502, L177
Xiong, D., & Deng, L. 2001, MNRAS, 327, 1137